

Self-Assembling Chains, Rings and Droplets in Dipolar Granular Fluids

Daniel L. Blair and A. Kudrolli

Department of Physics, Clark University, Worcester, MA 01610, USA

(December 18, 2019)

We visualize the distinct phases of magnetized steel particles thermalized by vibrations. A transition from a gas to clustered phase is observed as the granular temperature, is slowly decreased. Below the gas-cluster transition, structures spontaneously self-assemble and grow as the surrounding free particles are depleted to a saturation value determined by the temperature and volume fraction. Initially, these clusters are spatially compact, but grow linearly in time to form large extended droplets. If the system is quenched to low temperatures, a meta-stable network of connected chains is found. These results are consistent with both a classical nucleation process, and recent theories of entropic networks of dipolar hard spheres.

The nucleation of phases and the nature of phase transitions is of fundamental importance in understanding the liquid state of matter [1]. In fluids where particles interact isotropically, the van der Waals potential is very effective in describing both the structure and phase behavior. However, a considerable number of fluids such as ferrofluids and electro-rheological fluids, have strong anisotropic interactions. These fluids show complex phases depending on applied field and temperature [2]. In order to gain insight on the effects of anisotropy, the dipolar hard sphere model (DHSM) has been introduced and investigated. In spite of its simplicity, the mechanism for the nucleation of phases, and the very existence of a gas-liquid critical point, remains elusive. The interaction between two dipolar spheres separated by distance r is given by

$$U = U_{HS} + \frac{1}{r^3}(\vec{\mu}_i \cdot \vec{\mu}_j) - \frac{3}{r^5}(\vec{\mu}_i \cdot \vec{r}_{ij})(\vec{\mu}_j \cdot \vec{r}_{ij}), \quad (1)$$

where U_{HS} corresponds to the hard core repulsion interaction, $\vec{\mu}$ is the dipole moment, and \vec{r} is the interparticle vector connecting the centers of dipoles i, j .

Clearly from an energy point of view, neighboring particles like to align head to tail. If the potential is averaged over all of space, one gets a r^{-6} similar to a van der Waals liquid. Hence, one might naively expect phase separation into coexisting liquid and gas phases to occur [3,4]. However, early simulations of the DHSM did not find phase coexistence between the gas and liquid states but instead found chains of dipoles that are aligned head to tail [5]. It was therefore proposed that the weakly interacting chains preclude coexistence [6,7]. More recent large scale Monte Carlo simulations revealed the existence of liquid states, where chaining is greatly reduced and particles have high coordination number [8,9].

Building on these studies, Tlusty and Safran [10] have developed a topological model which investigates the critical liquid-gas transition. They have found phase coexistence as well as critical behavior by considering the concentration of threefold junctions and free ends. Experiments with magnetic colloidal suspensions appear to show aggregate droplets (clusters) that are much larger

than the size of a single particle in the liquid phase [11]. However, the effect of polydispersity and the role of electrostatic forces in the sample is unclear [12]. More recent experiments [13], based on static susceptibility measurements show a liquid phase even when the particle size distribution is fairly narrow. Because these observations are indirect, the structure of the clusters in the liquid is not known with certainty. Thus, it is clear that additional experiments, especially those that allow for visualization of structure and nucleation within all phases, are required to resolve the apparently contradictory results of indirect observations, simulations, and theory.

In this Letter, we present a simple macroscopic technique that allows for the investigation of the dipolar hard sphere model at finite temperature, from the perspective of attractive granular media. Using magnetic particles we are able to directly visualize the phases of thermalized hard spheres with embedded dipole moments. We find that the phase behavior is density and quench rate dependent.

Our experiments are inspired by granular physics [14]. Recently [15], systems of steel particles contained in vertically vibrated shallow containers were utilized to investigate the range over which kinetic theory [16] can be usefully applied to granular matter. Because the thermal energy scale is much smaller than the potential energy needed to raise a grain by its diameter, a new parameter called the “granular temperature” T has been introduced [17]. This temperature is defined as the mean fluctuation of the velocity of the granular particles and has been interpreted to be analogous to the usual temperature in thermal systems. In this geometry, the velocity distributions are found to be close to Gaussian [15,18].

The apparatus consists of a 30.0 cm diameter flat, anodized aluminum plate, with 1.0 cm sidewalls and a clear acrylic lid, that is weakly coupled through a rigid linear bearing to an electromechanical shaker. The system is leveled to within 0.001 cm to ensure that the plate is uniformly accelerated. The measured r.m.s. velocity of the plate $v_s = A\omega$, where A, ω are the amplitude and angular frequency, is varied between $v_s = 0.0 \rightarrow 7.0 \text{ cm s}^{-1}$ at $\omega = 377 \text{ rad s}^{-1}$ [see Fig. 1, and caption]. Image data

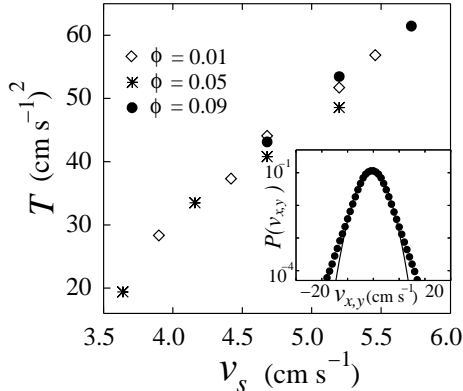


FIG. 1. Plot of granular temperature T , versus the r.m.s. velocity of the bottom plate of the container given by v_s . The data is essentially independent of ϕ . Each point represents the second moment of $P(v_{x,y})$ at three different values of ϕ . We utilize these points to relate T to v_s . (Inset) Example of a distribution $P(v_{x,y})$ of the components of the velocity in the x, y -plane at $\phi = 0.05$. The solid line is a fit to a Gaussian distribution. The deviations, measured by the kurtosis, are observed to be small, (3.11 as opposed to 3 for a Gaussian distribution).

is acquired through a high speed Kodak SR-1000 digital camera with a spatial (temporal) resolution of 512×480 pixels (250 f.p.s); we also utilize external triggering in order to perform time lapse. The particles used in the experiments are chrome steel spheres with a diameter of $\sigma = 0.3$ cm (with a high degree of sphericity $\delta\sigma/\sigma \sim 10^{-4}$) and mass $m = 0.12$ g. Each sphere has been placed in a ramped field of 1×10^4 G to embed a permanent moment of $\mu \sim 10^{-2}$ emu per particle. The covering fraction of magnetic particles, ϕ , is varied from $\phi = 0.01 \rightarrow 0.15$. We also place glass particles of equivalent mass, with a fixed volume fraction of $\phi_p = 0.15$ to introduce additional stochasticity into the system. The glass particles act as thermal carriers to ensure that as the magnetic particles condense, the temperature of the system does not go to zero.

The granular temperature T is measured from the velocity components of the magnetized particles, while in the gas phase, along the two horizontal axes $v_{x,y}$, and using $T = \langle v_{x,y}^2 \rangle$ which corresponds to the width of the velocity component distribution. The averaging is performed over all particles and over time. The $v_{x,y}$ -distributions [Fig. 1 inset] deviate from a Gaussian consistent with previous observations [15], but the deviations are not significant as measured by the fourth moment or the kurtosis of the distribution. Hence, the kinetic theory approach is still expected to apply in this case of weak dissipation [19].

Figure 2 shows typical examples of the kinds of self-assembled clusters present in our system. These structures appear when T is lowered below the value where single particles are able to link with other particles. The temperature at which long lived structures first appear is

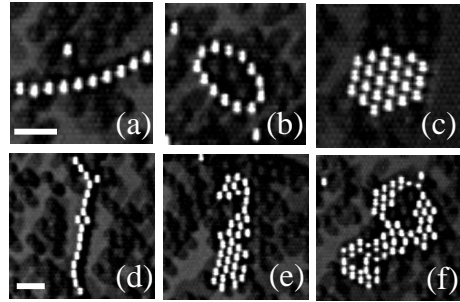


FIG. 2. Examples of chains (a), rings (b), and clusters (c) observed. Compact clusters appear to be the most stable configuration. (d – f) The evolution of a n-mer at $\phi = 0.05$, $T < T_s$ over 1080 s into a compact cluster. The scale bar on each set of images denotes 1 cm.

the transition temperature T_s , which depends on ϕ . As T_s is approached from above, the magnetic particles begin to cluster into short-lived dimers and trimers. These short chains are the seeds for the observed structures in Fig. 2(a–c).

We find that long chains are unstable, and in time will give way to more compact structures. Chains of length $\ell \geq 4$ particles will form either *ring* configurations, shown to be energetically favorable [3,20], or more stable configurations [see Fig. 2(b,c)]. There are at least two possible scenarios for the change from the chain configuration: (1) Chains are highly mobile. Mobility, due to the rotational and translational degrees of freedom, allow chains to align in head-to-tail droplets and grow through a coarsening process. (2) Due to the flexibility of the chains, their free ends, which have long-range attractive interactions, will eventually attach themselves to a particular part of the chain and form a loop or *closed Y* or find the other free end and form a ring [see Fig. 2(b)]. By calculating the energy gain due to the closure of a chain, it becomes clear that any chain of $\ell \geq 4$ is energetically unfavorable in comparison to a more compact configuration. We also find that rings are eventually “compressed” by the impinging *thermal* particles. The images in Fig. 2(d–f) show a time series for a particular chain at $T < T_s$. Initially, the chain [Fig. 2(d)] consists of the beginnings of a *Y* structure at the top and a ring of four particles in the center. Figure 2(e) shows an intermediate configuration, and Fig. 2(f) shows the cluster in Fig. 2(d,e) after 1080s that coexists with individual particles.

To characterize the transition from a gas-like phase that consists of single particles and short lived dimers and trimers to a more clustered phase consisting of extended droplets, we plot the phase diagram [Fig. 3(a)]. The connected line shows the transition temperature T_s as a function of ϕ . Above T_s , short lived dimers and trimers are observed along with single particles, but at and below this temperature, the clusters are observed to grow and not disassociate. Figure 3(b) shows an image of

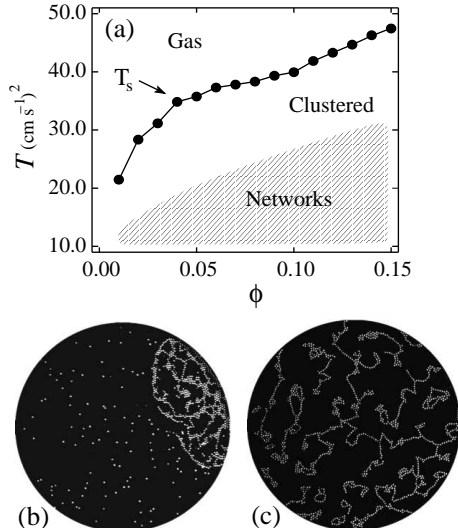


FIG. 3. (a) The phase diagram of temperature T versus the covering fraction of the particles ϕ . A gas phase consisting of single particles and short lived dimers and trimers are observed above a transition temperature T_s that depends on ϕ . Below T_s , dimers and trimers act as seeds to the formation of compact clusters that coexist with single particles. The transition from gas to compact clusters or droplets shows an apparent hysteresis. If T is rapidly quenched from the gas region to very low T highly ramified networks of particles form. (b) Snapshot of the system at $\phi = 0.09$, where $T \rightarrow T_s$ from the gas state after 1092 s. (c) The system at $\phi = 0.15$ after a rapid quench from the gas state into the network state.

the system with $\phi = 0.09$ after an initial seed in the shape of a ring has grown for 1092 s at T_s . If T is increased above T_s , droplets appear to be hysteretic. This hysteresis depends on the ramping rate of T , and is not observed to disappear over laboratory time-scales. Therefore it appears that the observed phase transition is first order. Within the clustered phase there exists a meta-stable network phase, shown by the shaded region. This phase [see Figure 3(c)], is attained by quenching to a T far below T_s from the gas state. This instantaneous quench produces a highly ramified mesh of particles. These networks show similarities to dipolar networks found in simulations and theory [8,10].

We next utilize the Hoshen-Kopelman [21] cluster identification algorithm to identify individual clusters formed at T_s , and then track their size, center of mass and radius of gyration. The average number of particles contained in a cluster $\langle n_c \rangle = n_c/n$, where n is total number of clusters formed, is plotted versus the radius of gyration R_g [Fig. 4(a)]. n is unity for most times, but may vary at very short times. This data was obtained for 1092 s immediately after T was lowered to T_s . Using the scaling relation $n_c \sim R_g^d$ [22], we measure the compactness of the clusters. Figure 4(a) clearly shows a crossover in the dimensionality of the clusters. Clusters with $R_g < 5.0\sigma$ follow closely to the spatial dimension. As the number

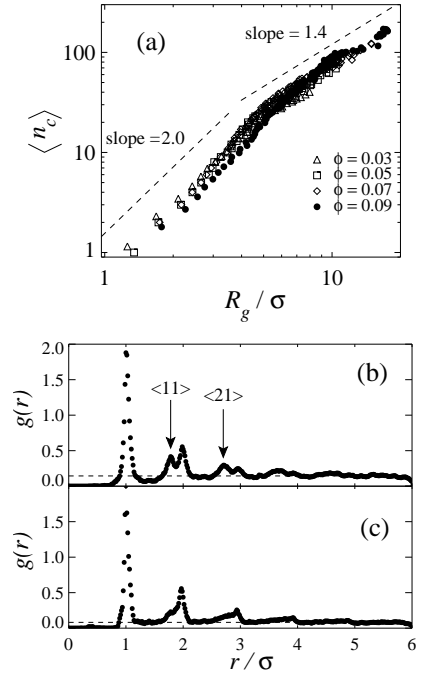


FIG. 4. (a) Average cluster size $\langle n_c \rangle$ versus the radius of gyration R_g/σ . The scaling $\langle n_c \rangle = \alpha R_g^d$, where $\alpha = \pi^2/2\sqrt{3}$, shows a crossover at $R_g \sim 5\sigma$ indicating that the clusters start more compact and become more extended. (b) The Spatial correlation function $g(r)$ versus r/σ for clusters formed at T_s after 1092 s at all ϕ , the arrows indicate the Miller indices discussed in the text. (c) $g(r)$ for the system in the networked phase at $\phi = 0.15$, at short times. The dashed lines indicate the average density of the clusters. The smearing of peaks in (c) compared to those in (b) shows that short range crystallization is suppressed in the network phase, indicating a liquid-like state.

of particles per cluster increases with time the trend for the fractal dimension, d , at all ϕ , is more consistent with $d = 1.4 \pm 0.1$. This implies that clusters are initially more compact and become more extended as they grow. If our system was composed of purely string-like objects d would take on a value near unity.

To further quantify the structure of the clusters, we use the spatial correlation function

$$g(r) = \frac{1}{2\pi r n_c} \sum_i^{n_c} \sum_{j=i+1}^{n_c} \delta(r_{ij} - r), \quad (2)$$

where r_{ij} is the distance between particles i and j . Figure 4(b) shows $g(r)$ versus r/σ for clusters after 1092 s at all ϕ , when $T = T_s$. The second and fourth peaks correspond to the Miller indices $\langle 11 \rangle$ and $\langle 21 \rangle$, respectively, that one would find in a 2D close-packing of spheres. This indicates that at small distances the clusters are close packed. However, if the system is quenched into the networked phase, by rapidly lowering T below T_s [see Fig. 3(c)], the short range order is removed as shown by the smoothing of secondary peaks in $g(r)$ [Fig. 4(c)]. The

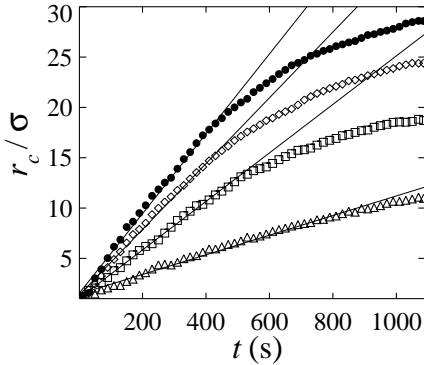


FIG. 5. The radial growth rate r_c/σ at $T = T_s$ for each ϕ . The solid lines are fits to the data over a time when the cluster is not in contact with the wall. The apparent crossover in growth rate is due to a finite size effect. Linear growth is consistent with a Wilson-Frenkel growth process, where individual hard spheres are absorbed onto the cluster. Symbols for each $\phi = 0.03$ (\triangle), 0.05 (\square), 0.07 (\diamond), and 0.09 (\bullet).

loss of orientational order and thus crystallinity implies the network phase may be considered a liquid-like phase, similar to liquids of entropic networks [10].

Next we plot the cluster growth rates by measuring the number of free particles at T_s for various ϕ . We find that the average radius r_c given by $n_c^{1/d}$ ($n = 1$ for Fig. 5 over all time) contained in a cluster grows linearly as the surrounding free particles are depleted to a saturation value determined by ϕ . The linear growth of crystal radii is consistent with the Wilson-Frenkel growth process of hard sphere colloidal crystals, where individual particles are absorbed onto the surface of a crystallite [23,24], although the mechanism is quite different. At low ϕ the growth of the cluster is near linear at all times [see Fig. 5]. As ϕ increases the linear growth gives way to an arrested growth rate. This slow down can also be explained by a finite size effect. For all data sets shown in Fig. 5 only clusters that nucleate close to the center of the cell are measured. Because the clusters are mobile they drift and move in the cell, and will eventually come to rest at the sidewall [see Fig 2(b)] due to depletion forces from the thermal particles [25]; this occurs at earlier times for higher ϕ . When this happens, half of the surface is not absorbing free particles, therefore the growth rate decreases.

In summary, we visualize the nucleation of the clustered phase in a dipolar hard sphere system by using magnetized steel particles. This allows for a direct investigation into the nature of the clusters formed. The self-assembled clusters initially compact but become extended as they grow and coexist with the gas phase. A networked phase is observed if the system is rapidly cooled. This phase is very similar entropic networks, discussed recently [10], but appears to be a metastable state.

We thank C. Landee, H. Gould, G. Johnson, L.

Colonna-Romano and T. Tlusty for fruitful discussions. This work was partially supported by National Science Foundation under Grant # DMR-9983659 and Alfred P. Sloan Foundation.

- [1] D. Chandler, J. D. Weeks, and H. C. Anderson, *Science* **220**, 787 (1983), and the references contained within.
- [2] R. E. Rosensweig, *Ferrohydrodynamics* (Cambridge University Press, Cambridge, 1985).
- [3] P. G. deGennes and P. A. Pincus, *Phys. Kondens. Mater.* **11**, 189 (1970).
- [4] Y. Levin, *Phys. Rev. Lett.* **83**, 1159 (1999).
- [5] M. E. van Leeuwen and B. Smit, *Phys. Rev. Lett.* **71**, 3991 (1993).
- [6] R.P. Sear, *Phys. Rev. Lett.* **76**, 2310 (1996).
- [7] R. van Roij, *Phys. Rev. Lett.* **76**, 3348 (1996).
- [8] P. J. Camp, J. C. Shelley, and G. N. Patey, *Phys. Rev. Lett.* **84**, 115 (2000).
- [9] P. Rein ten Wolde, D. W. Oxtoby, and D. Frenkel, *J. Chem. Phys.* **111**, 4762 (1999).
- [10] T. Tlusty and S. A. Safran, *Science* **290**, 1328 (2000).
- [11] H. Wang, *et al.*, *Phys. Rev. Lett.* **72**, 1929 (1994).
- [12] P. Linse and V. Lobaskin, *Phys. Rev. Lett.* **83**, 4208 (1999).
- [13] H. Mamiya, I. Nakatani, and T. Furubayashi, *Phys. Rev. Lett.* **84**, 6106 (2000).
- [14] H. Jaeger, S. Nagel, and R. P. Behringer, *Rev. Mod. Phys.* **68**, 1250 (1996).
- [15] W. Losert, D. Copper, J. Delour, A. Kudrolli, and J. P. Gollub, *Chaos* **9**, 682 (1999); J. S. Olafsen and J. S. Urbach, *Phys. Rev. E* **60**, R2468 (1999).
- [16] P. K. Haff, *J. Fluid Mech.* **134**, 401 (1983); J. T. Jenkins and S. B. Savage, *J. Fluid Mech.* **130**, 187 (1983).
- [17] S. Ogawa, in *Proc. US - Japan Semin. Contin-Mech. and Stat. Approaches Mech. Granular Mater.* (Gukujutsu Bunken Fkyakai, Tokyo, 1978), p. 208.
- [18] A. Kudrolli and J. Henry, *Phys. Rev. E* **62**, R1489 (2000); F. Rouyer and N. Menon, *Phys. Rev. Lett.* **85**, 3676 (2000); D. L. Blair and A. Kudrolli, *Phys. Rev. E* **64**, 050301 (2001).
- [19] A. Puglisi, V. Loreto, U. M. Marconi, A. Petri, and A. Vulpiani, *Phys. Rev. Lett.* **81**, 3848 (1998); T. P. C. van Noije and M. H. Ernst, *Granular Matter* **1**, 57 (1998).
- [20] W. Wen, F. Kun, K. F. Pál, D. W. Zheng, and K. N. Tu, *Phys. Rev. E* **59**, R4758 (1999).
- [21] J. Hoshen and R. Kopelman, *Phys. Rev. B* **14**, 3438 (1976).
- [22] $n_c = \alpha R_g^d$, where α is determined by the dimensionality and mass elements. We are 2D and use spheres (disks), therefore $\alpha = \pi^2/2\sqrt{3}$.
- [23] B. J. Ackerson and K. Schätzel, *Phys. Rev. E* **52**, 6448 (1995).
- [24] U. Gasser, E. R. Weeks, A. S. Schofield, P. N. Pusey, and D. A. Weitz, *Science* **292**, 258 (2001).
- [25] P. D. Kaplan, J. L. Rouke, A. G. Yodh, and D. J. Pine, *Phys. Rev. Lett.* **72**, 582 (1994).